HiExM: high-throughput expansion microscopy enables scalable super-resolution imaging

John H. Day[1], Pema Maretich[2#], Catherine Marin Della Santina[1#], Alexander L. Auld[2#], Tay Shin[3], Edward S. Boyden[1,3,4,5,6,7,8,9], Laurie A. Boyer[1,2*]

[1]Department of Biological Engineering, [2]Department of Biology, [3]Department of Media Arts and Sciences, [4]Department of Brain and Cognitive Sciences, [5]McGovern Institute, [6]Howard Hughes Medical Institute, [7]K Lisa Yang Center for Bionics, [8]Center for Neurobiological Engineering, [9]Koch Institute, Massachusetts Institute of Technology, 77 Massachusetts Avenue, Cambridge, MA 02139 USA

#These authors contributed equally.

*Correspondences:
Laurie A. Boyer
lboyer@mit.edu
Tel: +1 617 324-3335

Key words: expansion microscopy, high-throughput, nanoscopy, super-resolution imaging

ABSTRACT

Expansion microscopy (ExM) involves the physical, isotropic expansion of specimens enabling nanoscale imaging using a standard confocal microscope. ExM is widely employed to image proteins, nucleic acids, and lipid membranes in single cells at nanoscale; however, current methods are low throughput which limits the number of samples that can be processed simultaneously. We developed High-throughput Expansion Microscopy (HiExM), a robust platform that enables expansion microscopy of cells cultured in a standard 96-well plate. Our method enables consistent ~4.2x expansion across individual wells and entire plates in parallel. We also demonstrate that samples expanded using HiExM can be imaged and analyzed using standard high-throughput confocal imaging platforms. Our method broadens the application of ExM as a tool for scalable super-resolution imaging of specimens for pharmaceutical and research applications including drug and cell phenotype screening.

The ability to resolve subcellular features can greatly enhance biological discovery, identification of disease targets, and the development of therapeutics. Super resolution microscopy methods such as structured illumination microscopy (SIM), electron microscopy (EM), stochastic optical reconstruction microscopy (STORM) and photoactivated localization microscopy (PALM) enable nanoscale imaging of specimens.[1,2,3] However, these approaches require specialized, costly reagents and microscopes. Expansion microscopy (ExM) is an alternative, inexpensive and accessible method that similarly resolves fluorescently labeled structures at subcellular resolution by isotropically enlarging specimens within a swellable polyelectrolyte hydrogel.[4] Images of expanded cells show a higher effective resolution due to an increase in the distance between the fluorescent molecules beyond the Rayleigh limit typical of a conventional confocal microscope. Super-resolution imaging and ExM are critical tools that are widely used in biological research; however, processing and sample imaging requires time consuming manual manipulation limiting its throughput. Although there has been success in increasing the throughput of certain super-resolution microscopy techniques, these methods still require highly specialized equipment and expertise which limits their application.[5,6,7] To broaden the utility and ease of use of super-resolution imaging, we developed High-Throughput Expansion Microscopy (HiExM) that combines parallel sample processing and automated high-content confocal imaging in a standard 96-well cell culture plate.

Adapting standard ExM to a 96-well plate requires the reproducible delivery of a small volume of gel solution to each well (<1 μL compared to ~200 μL for standard ExM). This small volume allows complete gel expansion within the size constraints of wells in a 96-well plate. To achieve this goal, we engineered a device that retains small liquid droplets when dipped into a reservoir of expansion gel solution. These droplets can then be deposited into the center of multiple wells of the culture plate (**Figs. 1a,b**). The retention of the gel solution is mediated by a series of reticulated grooves at the end of a cylindrical post which favors the formation of a pendant droplet (**Fig. 1c**). We estimate that each post retains ~230 nL of gel solution as measured by the mass of liquid accumulated on all post tips of a single device after dipping (Supplementary Methods). Visual inspection of the droplets deposited by the device indicated a uniform distribution of gel solution within the wells.

Delivery of the gel solution in each well allows for formation of a toroidal gel where the inner surface is molded by the conical surface of the post-tip and the outer surface of the gel is

constrained by surface tension (**Figs. 1c,d**). As such, the post-tip dimensions were designed to deliver a volume of gel solution that would maximally expand to the diameter of the well (**Fig. 1d**). We reasoned that a toroidal gel would allow for isotropic gel expansion within the well constraints while allowing for easy device removal because the inner surface of the gel expands outward away from the conical post-tip, effectively detaching the gel from the device. To achieve this toroidal geometry, we incorporated a compliant mechanism composed of three key features that allows each post of the device to contact the midpoint at the bottom of a well (**Fig. S1**). First, two sets of three cantilevers (termed 'pressure struts') are located at each end of the device while the remainder consists of two rows of 6 posts (12 posts per device). These pressure struts apply outward force to the inside of the outer four wells ensuring that the device remains in contact with the well surface throughout the expansion process. Second, the spine of the device incorporates several notches extending through the long side of the device allowing it to bend to accommodate inconsistencies between the depths of individual wells. Finally, the post lengths are offset from the center four posts out to allow for sequential deformation that ensures each post contacts the well surface. Together, these design features allow for reproducible deposition and expansion of gels in a 96-well plate.

To test our device for high-throughput gel expansion, we first performed standard expansion microscopy using ammonium persulfate (APS) and tetramethylethylenediamine (TEMED) to initiate gel polymerization (**Fig. S2a**).[8] Since APS rapidly accelerates polymerization of polyacrylamide hydrogels, TEMED-containing expansion gel solution is first delivered by the device and removed leaving a ≤1μl droplet in each well of the plate on ice. A second device is then used to deliver APS-containing expansion gel solution at the same volume and the polymerization reaction is initiated by exposing the plate to heat. Given the large air-liquid-interface in the well plate, droplet delivery and polymerization are performed in a nitrogen filled glove bag to minimize oxygen inhibition of the reaction. Although we observed gel formation across wells, polymerization and expansion were inconsistent, likely due to inhomogeneous radical formation and rapid evaporation relative to the rate of polymerization (**Movie S1**). To overcome this limitation, we tested photochemical initiators including Lithium phenyl(2,4,6-trimethylbenzoyl)phosphinate (LAP), diphenyl(2,4,6-trimethylbenzoyl)phosphine oxide (TPO), and 1-[4-(2-Hydroxyethoxy)-phenyl]-2-hydroxy-2-methyl-1-propane-1-one (Irgacure 2959) which have been used to control polymerization of polyacrylamide gels when exposed to UV light.[9,10,11] LAP has previously shown success in slide-based ExM using PEG hydrogels.[12] We found that

using Irgacure 2959 resulted in highly reproducible gel formation and expansion (**Movie S2**) in our platform compared to other photoinitiators tested or standard ExM chemistry.

We next tested whether our HiExM platform could achieve nanoscale image resolution of biological specimens. Briefly, A549 cells were cultured, fixed, permeabilized and immunostained with alpha-tubulin antibodies to visualize microtubules as a reference structure before and after expansion. Stained samples were then incubated with Acryloyl X (AcX) overnight at 4ºC to allow anchoring of native proteins to the polymer matrix during gel formation. Device posts were immersed in the expansion gel solution containing 0.1% Irgacure 2959. The devices were then inserted into the well plate followed by exposure to UV light (365nm) in an anoxic environment to initiate the polymerization reaction. Resulting gels were then digested with Proteinase K followed by expansion in deionized water overnight (**Fig. S2a**; see Methods). Visual inspection using an epifluorescence microscope indicated both robust gel formation and fluorescence signal retention across wells. Although we observed photobleaching in our photopolymerized gels initiated with Irgacure 2959 when staining with AlexaFluor® dyes, we found that Cyanine-based Fluorescent (CF®) dyes are robust against bleaching in HiExM and result in reproducible signal retention (**Fig. S3**).[13]

A major workflow bottleneck associated with super resolution imaging, including current ExM protocols, is the time and expertise required for image acquisition. For example, the vertical component of expansion makes it difficult to image the full depth of the sample. Moreover, expansion gels are not bound to the well surface following digestion in our system, which requires increasing the search space for planar coordinates and focal depths to fully image the expanded specimen. To enable simultaneous 3D image capture and data acquisition of expanded gels in 96-well plates, we performed image analysis using a high content confocal microscope (Opera Phenix system, Perkin Elmer) (**Fig. 2a**). This approach allowed autonomous capture of images of individual cells and wells across the entire plate at a resolution of ~115 nm compared to ~463 nm for unexpanded samples with the same microscope, objective (63X, 1.15NA water immersion), and imaging wavelength (**Fig. S4**).

We next benchmarked the performance of our platform relative to slide-based proExM. We first measured image distortion from expansion using a non-rigid registration (NRR) algorithm.[4] Prior to expansion, images of stained A549 cells were acquired using the Opera Phenix from 61 fields

around the center of each gel (**Fig. 2a**). Cells were then expanded as described above and 12 fields were imaged per well. Distortion was calculated using the root mean squared error (RMSE) of a 2-dimensional deformation vector field by comparing microtubule morphology in the same cell(s) before and after expansion in six to ten fields in each well across six arbitrarily selected wells (**Figs. 2c,d**). The average percent error (up to 40 μm measurement length post-expansion) was plotted against the distance from the center of the gel (**Fig. 2e**). Our analysis found no correlation (R^2 = 0.003) between expansion error and distance from the gel center. In fact, we observed only a single or small number of outliers (>3 s.d.) in any given well (<2 instances per gel of 6 gels tested). These outliers are not expected to affect biological interpretation. These outliers, which are closer to the center of the gel, likely occur when the device post is not in full contact with the well surface, resulting in a higher volume of gel at the center of the toroid that resists gel swelling under the device (**Fig. S5**). Moreover, expansion was highly consistent when comparing wells across multiple plates, showing minimal error (average = 3.68%) comparable to slide-based ExM (**Fig. 2f**).[4,8] In fact, we observed only a small number of image fields (7 of 58) with error above 6% (maximum 6.78%). We also calculated error across gels using APS and TEMED polymerization chemistry and found that photoinitiation resulted in markedly lower spatial errors in our platform (**Fig. S6**). Analysis of expansion at different cell seeding densities also showed that cell confluency did not result in significant difference in image distortion as measured by NRR (**Fig. S7**).

Finally, we measured expansion factors within individual gels, between gels, and across plates by manually measuring the distance between pairs of cell landmarks in FIJI before and after expansion. We found that the expansion factor was highly reproducible across different regions of the gel confirming robust expansion using our method (**Fig. 2g**). Moreover, the average expansion factor of wells sampled across three plates was 4.16 +/- 0.394 (**Fig. 2h**), consistent with ProExM.[8] Collectively, these data indicate that our HiExM method results in reproducible nanoscale and isotropic expansion of cells within gels, across wells and plates.

HiExM robustly reproduces the three-dimensional structure of pre-expansion cells at nanoscale resolution allowing for processing and autonomous imaging in a 96-well cell culture plate. Our simple and inexpensive workflow also allows for simultaneous processing of multiple plates, greatly extending the throughput of super-resolution imaging. Moreover, adapting ExM to conventional 96-well cell culture plates allows the user to analyze cells under a range of conditions

and time points. Thus, HiExM can enable large scale biological and pharmaceutical applications that would benefit from nanoscale spatial resolution including cell phenotyping as well as drug and toxicology screening.

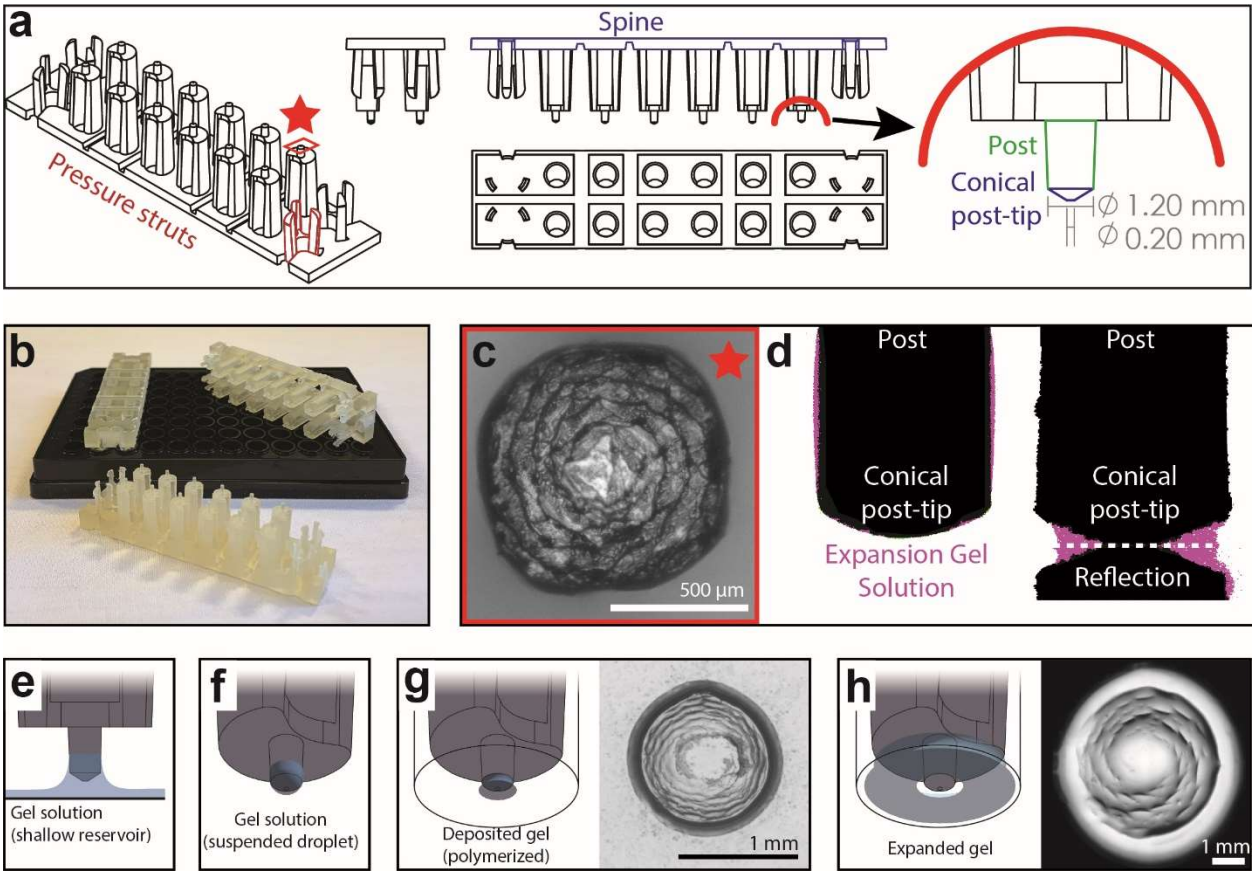

Fig. 1. HiExM enables gel formation and expansion in a 96-well cell culture plate. a. Schematic representation of HiExM devices showing the key features highlighted in color. **b.** Example devices used in 96-well cell culture plates. The device on the left is inserted into the well plate. **c.** Brightfield image of the conical post-tip shows the pattern of grooves that mediate fluid retention. **d.** Fluid retention at the conical post-tip of the device. Silhouettes taken by an optical comparator of the profile of a single post suspended above a surface (left) and in contact with a surface (right) show a fluid droplet interacting with the device. Upon device insertion, the gel solution fills the space under the conical post tip, forming the toroid gel. **e-h.** Schematic of HiExM gel deposition and expansion workflow. **e.** The device is immersed in a shallow reservoir of gel solution. **f.** Upon removal, the tip of each device post retains a small volume of gel solution. **g.** Gel solution is deposited by the device into the centers of each well of the cell culture plate.

Brightfield image (right) shows gel geometry and size prior to expansion. **h.** Polymerization and expansion are carried out with the device in place. Brightfield image (right) shows gel geometry and size after expansion.

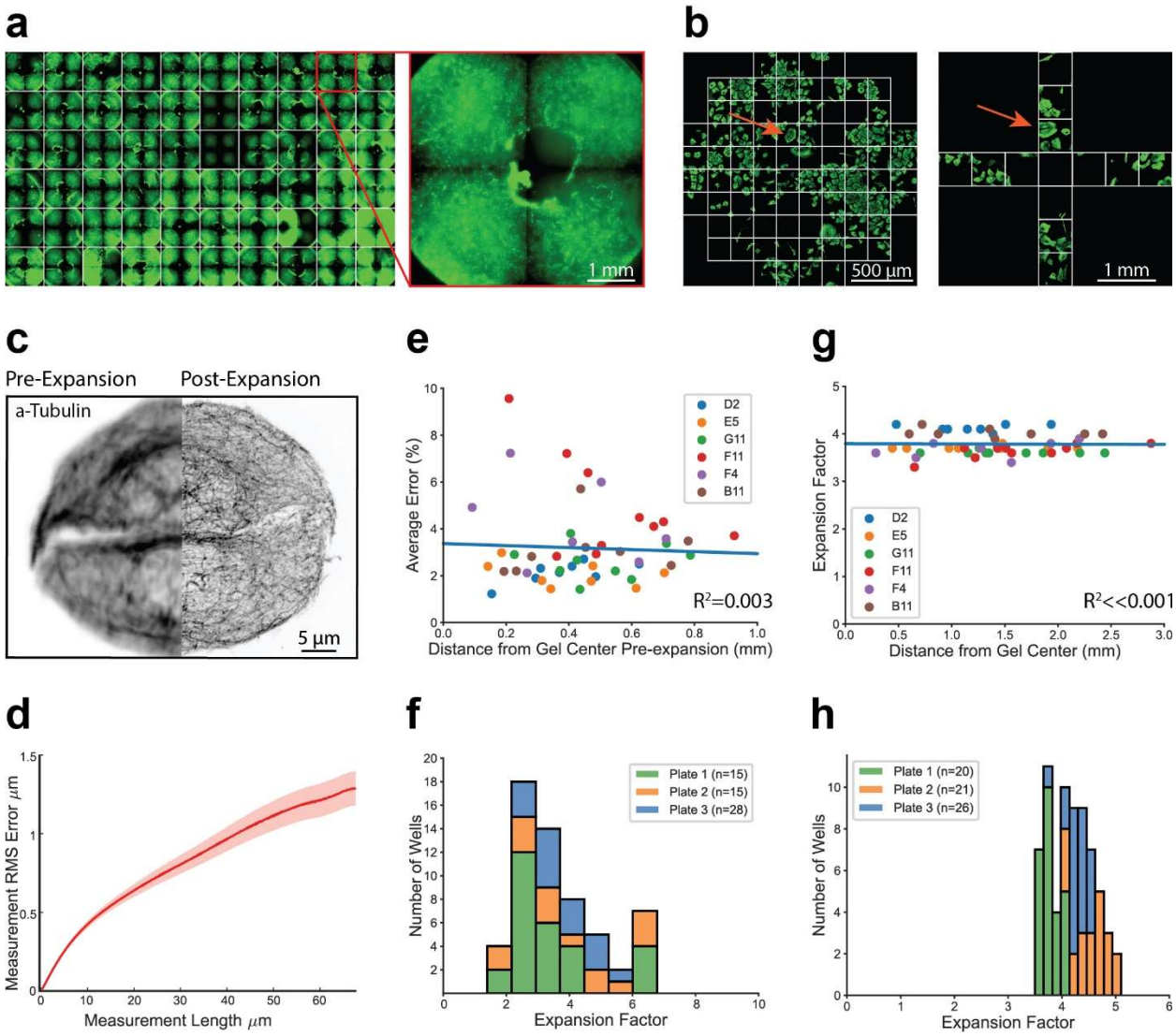

Fig 2. HiExM is compatible with nanoscale expansion and automated image acquisition of human cells with minimal distortion. a. Expanded gels in a 96 well plate imaged at 5x with an inset showing an individual gel. **b.** Imaging fields for pre-expansion and post-expansion data acquisition. Prior to expansion, 61 fields were imaged at 63x around the center of the gel. After expansion, 12 fields were imaged at 20x magnification. Max projections for each field were then stitched together and manually inspected to identify fields in the pre-expansion and post-expansion image sets containing matching cells. Arrows show an example of a field representing

the same pair of cells before and after expansion. **c.** Representative registered fluorescence image of microtubules before (left) and after (right) expansion showing the increase in resolution conferred by expansion. **d.** Representative error curve calculated using non-rigid registration on 43 independent fields of view. The shaded region denotes one standard error of the mean. **e.** Error is not dependent on the location of a given field of view within the gel. Each data point represents the average percent error (up to 40 μm measurement length post-expansion) for a given field of view as determined by an NRR analysis. Six wells were analyzed in seven to ten fields of view. The distance from the center of each field of view to the center of the well was measured manually in FIJI using the stitched pre-expansion image set. **f.** Stacked-bar histogram showing the distribution of average error among gels across three plates (average = 3.63% +/- 1.39). Average error percentages for each well plate: 3.73 +/- 0.879, 3.89 +/- 1.65, and 3.43 +/- 1.44. **g.** Expansion factor is not dependent on the location of a given field of view within the gel. Images taken before and after expansion of the same cell or group of cells were used to measure the ratio of length scales in the two images. **h.** Stacked-bar histogram showing the distribution of expansion factors in 58 gels across three plates. Expansion factors ranged from 3.5-5.1x across gels with an average of 4.16 +/- 0.394. Average expansion factors for each well plate: 3.78 +/- 0.171, 4.26 +/- 0.171, and 4.53 +/- 0.321.

MATERIALS AND METHODS

Cell culture

Human A549 cells were maintained in culture at a density between $2x10^3$ and $1x10^4$ cells/cm^2 in DMEM modified with 10% fetal bovine serum and 1% penicillin-streptomycin. Glass and plastic 96-well plates were seeded at ~$1x10^4$ and $7x10^4$ cells/cm^2 for expansion experiments.

Immunofluorescence

Briefly, cells were fixed with 4% PFA for 15 minutes at room temperature and then blocked (1% bovine serum albumin and 0.1% Triton X100 in PBS) for one hour. Cells were then incubated for one hour at 37˚C with alpha-Tubulin antibodies (MilliporeSigma T5168) in a staining solution (0.1% bovine serum albumin and 0.1% Triton X100 in PBS) followed by incubation with secondary antibodies in staining solution for 1hr at 37C. Cells were washed between each stage in PBS three times for 10 minutes.

Primary Antibodies	Vendor	Cat. Number
Monoclonal anti-alpha-Tubulin antibody	MilliporeSigma	T5168
Secondary Antibodies	Vendor	Cat.Number
CF633 Chicken Anti-Mouse IgG (H+L)	Biotium	20222-1
Alexa Fluor 488 goat anti-mouse IgG (H+L)	Invitrogen	A11029
Alexa Fluor 546 donkey anti-goat IgG (H+L)	Invitrogen	A11056

HiExM Device Fabrication

HiExM devices were fabricated from polysulfone (McMaster-Carr 86735K74) using a Trak DPM2 CNC milling machine.

HiExM Workflow

Cells were fixed with 4% paraformaldehyde (PFA) and immunostained as described above and treated with Monomer solution (6-((Acryloyl) amino) hexanoic acid, abbreviated AcX) (Invitrogen A20770) overnight at 4C. Cells were then washed twice with PBS, once with DI water, and the remaining liquid was gently aspirated from the wells. Gel solution composed of 4.04M sodium acrylate (AK Scientific R624), 0.506M acrylamide (MilliporeSigma A4058), 0.00934M n, n'-methylenebisacrylamide (MilliporeSigma M1533), 1.84M sodium chloride (Invitrogen AM9759) and 1.45X PBS 1mL (Invitrogen AM9625) was prepared in a light-protected tube. 1-[4-(2-Hydroxyethoxy)-phenyl]-2-hydroxy-2-methyl-1-propane-1-one (Irgacure 2959, MilliporeSigma 410896) was dissolved in DMSO at a concentration of 1.64M and this solution was mixed into the gel solution for a final Irgacure 2959 concentration of 0.0328M. The HiExM protocol was performed in a glove bag purged two times with dry nitrogen (MilliporeSigma Z530112). The gel solution was poured onto an absorbent pad to form a fluid reservoir. Devices were dipped into the

gel solution and immediately inserted into the well plate. The plate was then irradiated for 60 seconds with UVA light using a Uvitron Portaray curing lamp placed 20 inches beneath the plate (Uvitron International UV2270). Approximately 100 µL of Proteinase K (NEB P8107S) digestion solution was added to each gel-containing well and incubated for ~6 hours at room temperature. After digestion, the 96-well plate was submerged in ~2 liters of DI water overnight under constant agitation while the gels were held in place by the device. Finally, the plate was removed from the water bath and devices removed from the well plate for imaging.

Image Acquisition

Confocal imaging was performed on an Opera Phenix imaging system (PerkinElmer). For NRR analysis, pre-expansion images were acquired with a 63x water objective (NA 1.15) in stacks of 6 planes spaced 0.5 microns apart and post-expansion images of the same plate were acquired using a 20x water objective (NA 1.0) in stacks of 50 planes spaced one micron apart. Prior to expansion, 61 tiled fields at the center of each well were imaged at 63x to capture cells that would be incorporated into the gel. After expansion, 12 fields in a cross pattern were imaged at 20x to capture a representative set of images for each gel across multiple wells. Movies S1 and S2 were obtained on an EVOS M5000 epifluorescence microscope (ThermoFisher Scientific).

Image analysis

Non-rigid registration

Non-rigid registration was performed to measure isotropic expansion within individual gels and across gels. For analysis represented in Fig. 2d, all fields of view were used in which a cell or group of cells could be identified in both the pre-expansion and the post-expansion image sets. The distance from the center of the analyzed field of view to the center of the well was measured in the pre-expansion image set. For Fig. 2f, a single field of view near the periphery of the gel was arbitrarily chosen to represent the whole gel. Non-rigid registration was performed using a custom MATLAB analysis pipeline as described.[4] Briefly, pre and post expansion images are coarsely aligned using the TurboReg plugin for ImageJ.[14] This pair of outputs is then histogram normalized and masks are generated to exclude regions with no features by applying a gaussian blur. B-spline-based registration package in MATLAB was used to do non-rigid registration between the images. This procedure was done on image fields measuring 400px x 400px for all analyses.

The resulting data from a non-rigid registration analysis is a curve that represents measurement error as a function of measurement length. To synthesize these curves into single points (as represented in Figs. 2c-f), The average percent error up to 40 μm measurement length (as measured after expansion) was used. The average percent error was found as the mean of the ratios of error to measurement length for each individual data point in the error curve up to 40 μm measurement length.

Expansion Factor

To calculate expansion factors, images taken before and after expansion of the same cell or group of cells were compared. In both images, the distance between two easily identifiable features was measured manually in FIJI, and the ratio of those measurements was used to calculate the expansion factor.

ACKNOWLEDGEMENTS

We thank Paul Tillberg and members of the Boyer and Boyden labs, especially Shiwei Wang, Chi Zhang and Asmamaw Wassie for helpful discussions. We also thank the Edgerton Student Shop and Mark Belanger for assisting in the fabrication of devices. This material is based upon work supported by the National Science Foundation Graduate Research Fellowship under Grant No. 2141064 and 1122374 to JHD and TS, respectively. This work is supported by NIH EB024261, NIH 1R01AG070831, HHMI, NIH 1R01MH123403, NIH R01MH124606, and NIH 1R56AG069192 to ESB. ESB acknowledges funding from Lisa Yang, Lore McGovern and John Doerr. This work is also supported by funding from the Leila and Harold G. Mathers Foundation, John J. Jarve Seed Fund and the Deshpande Center to LAB.

ESB is an inventor on multiple patents related to expansion microscopy, and co-founder of a company exploring commercial applications of expansion microscopy. JHD, PM, CMDS, ALA, ESB, and LAB are inventors on a provisional patent filed for HiExM.

LITERATURE CITED

1. Heintzmann, R. & Huser, T. Super-Resolution Structured Illumination Microscopy. *Chem. Rev.* **117**, 13890–13908 (2017).
2. Egerton, R. F. *Physical Principles of Electron Microscopy*. (Springer International Publishing, 2016). doi:10.1007/978-3-319-39877-8.
3. Henriques, R., Griffiths, C., Hesper Rego, E. & Mhlanga, M. M. PALM and STORM: Unlocking live-cell super-resolution. *Biopolymers* **95**, 322–331 (2011).
4. Chen, F., Tillberg, P. W. & Boyden, E. S. Expansion microscopy. *Science* **347**, 543 (2015).
5. Holden, S. J. *et al.* High throughput 3D super-resolution microscopy reveals *Caulobacter crescentus* in vivo Z-ring organization. *Proc. Natl. Acad. Sci. U.S.A.* **111**, 4566–4571 (2014).
6. Gunkel, M., Flottmann, B., Heilemann, M., Reymann, J. & Erfle, H. Integrated and correlative high-throughput and super-resolution microscopy. *Histochem Cell Biol* **141**, 597–603 (2014).
7. Mahecic, D. *et al.* Homogeneous multifocal excitation for high-throughput super-resolution imaging. *Nat Methods* **17**, 726–733 (2020).
8. Tillberg, P. W. *et al.* Protein-retention expansion microscopy of cells and tissues labeled using standard fluorescent proteins and antibodies. *Nat Biotechnol* **34**, 987–992 (2016).
9. Li, N., Xiang, Z., Rong, Y., Zhu, L. & Huang, X. 3D Printing Tannic Acid-Based Gels via Digital Light Processing. *Macromolecular Bioscience* **22**, 2100455 (2022).
10. Pawar, A. A. *et al.* High-performance 3D printing of hydrogels by water-

dispersible photoinitiator nanoparticles. *Sci. Adv.* **2**, e1501381 (2016).

11. Kuliasha, C. A. *et al.* Engineered Chemical Nanotopographies: Reversible Addition–Fragmentation Chain-Transfer Mediated Grafting of Anisotropic Poly(acrylamide) Patterns on Poly(dimethylsiloxane) To Modulate Marine Biofouling. *Langmuir* **36**, 379–387 (2020).

12. Blatchley, M. R. *et al.* In Situ Super-Resolution Imaging of Organoids and Extracellular Matrix Interactions via Phototransfer by Allyl Sulfide Exchange-Expansion Microscopy (PhASE-ExM). *Advanced Materials* **34**, 2109252 (2022).

13. Jiang, J., Li, X., Mao, F., Wu, X. & Chen, Y. Small molecular fluorescence dyes for immunocell analysis. *Analytical Biochemistry* **614**, 114063 (2021).

14. Thevenaz, P., Ruttimann, U. E. & Unser, M. A pyramid approach to subpixel registration based on intensity. *IEEE Trans. on Image Process.* **7**, 27–41 (1998).